Tissue biodistribution and blood clearance rates of intravenously administered carbon nanotube radiotracers

Ravi Singh*†, Davide Pantarotto*†‡§, Lara Lacerda*, Giorgia Pastorin‡, Cédric Klumpp‡§, Maurizio Prato§, Alberto Bianco‡, and Kostas Kostarelos*¶

*Centre for Drug Delivery Research, School of Pharmacy, University of London, London WC1N 1AX, United Kingdom; ‡Institut de Biologie Moléculaire et Cellulaire, Unité Propre de Recherche 9021, Centre National de la Recherche Scientifique, Immunologie et Chimie Thérapeutiques, 67084 Strasbourg, France; and §Dipartimento di Scienze Farmaceutiche, Università di Trieste, 34127 Trieste, Italy

Carbon nanotubes (CNT) are intensively being developed for biomedical applications including drug and gene delivery. Although all possible clinical applications will require compatibility of CNT with the biological milieu, their *in vivo* capabilities and limitations have not yet been explored. In this work, water-soluble, single-walled CNT (SWNT) have been functionalized with the chelating molecule diethylentriaminepentaacetic (DTPA) and labeled with indium (^{111}In) for imaging purposes. Intravenous (i.v.) administration of these functionalized SWNT (*f*-SWNT) followed by radioactivity tracing using gamma scintigraphy indicated that *f*-SWNT are not retained in any of the reticuloendothelial system organs (liver or spleen) and are rapidly cleared from systemic blood circulation through the renal excretion route. The observed rapid blood clearance and half-life (3 h) of *f*-SWNT has major implications for all potential clinical uses of CNT. Moreover, urine excretion studies using both *f*-SWNT and functionalized multiwalled CNT followed by electron microscopy analysis of urine samples revealed that both types of nanotubes were excreted as intact nanotubes. This work describes the pharmacokinetic parameters of i.v. administered functionalized CNT relevant for various therapeutic and diagnostic applications.

nanomedicine | blood circulation half-life | drug delivery | pharmacokinetics | nanotoxicology

Carbon nanotubes (CNT) represent the structural evolution of the archetypal molecular architecture consisting of pure carbon units, the C_{60} fullerene (1). CNT, or "buckytubes" (2, 3), possess extraordinary properties, including high electrical and thermal conductivity, great strength, and rigidity, and are being developed for a wealth of applications, including field emission (4), energy storage (5), molecular electronics (6–8), and atomic force microscopy (9). CNT have proven difficult to solubilize in aqueous solutions, limiting their use in biological applications. One of the most commonly used strategies to render CNT soluble in aqueous media, and therefore, potentially useful to biomedical applications, is through their surface functionalization (9, 10). The biomedical applications of CNT are still in their exploratory stage; however, significant promise has been shown (11). Such applications include their use as DNA biosensors (12), protein biosensors (13) and transporters (14), or ion channel blockers (15).

We have previously demonstrated that peptide-functionalized CNT are capable of penetrating the mammalian plasma membrane and translocating to the cell nucleus (16) and that these nanotubes are capable of eliciting an antigen-specific neutralizing antibody response *in vivo* (17). More recently, we reported the first case of CNT-mediated intracellular delivery of plasmid DNA using ammonium-functionalized single-walled CNT (SWNT-NH$_3^+$) leading to gene expression levels up to 10-fold that of naked DNA alone (18). These observations pave the way for the use of CNT as delivery systems for therapeutic and diagnostic molecules. In view of such biomedical applications of functionalized CNT (*f*-CNT),

their *in vivo* behavior needs to be identified. It is imperative to determine two equally important *in vivo* parameters before any clinical application of CNT can be deemed feasible, namely their toxicological and pharmacological profiles.

Elucidating the *in vivo* pharmacological profiles of administered CNT is considered very important in the context of the underlying medical debate regarding the safety of novel nanomaterials. The harmful effects of nanotubes, because of their nanoscale dimensions and carbon backbone, may arise from their capability to readily enter the respiratory tract (portal of entry), deposit in the lung tissue, redistribute from their site of deposition, escape from the normal phagocytic defenses, and modify the structure of proteins. In such ways, nanotubes can potentially activate inflammatory and immunological responses, affecting normal organ function. Recently, a number of studies have examined the toxicological profile of CNT and other fullerene-based nanostructures *in vivo* (19–26). Most of the CNT cytotoxicity studies have focused on the pulmonary toxicity after inhalation (20), intratracheal instillation (22, 23), and pharyngeal aspiration (24), as well as their effects on skin toxicity after exposure of skin to CNT (19, 21), and subcutaneous (s.c.) administration (25, 26), reporting acute pulmonary toxicity effects, induction of granulomas, and inflammatory reactions to the CNT. However, all of these studies used pristine, nonfunctionalized CNT, usually dispersed in an aqueous buffer with the aid of a surfactant such as Tween 80 (23).

A very recent report looked at the toxicity profile of acid-treated CNT of two different lengths (220 and 825 nm) s.c. administered to rats and reported no severe inflammatory response such as necrosis, tissue degeneration, or neutrophil infiltration (26). As has been reported for fullerenes and CNT, functionalization and the ensuing improvements in the aqueous solubility, and, therefore, biocompatibility of these materials, improve dramatically the toxicity profile observed *in vitro* (27, 28). Previously we reported that the water-soluble *f*-CNT used in the present study also exhibited a favorable *in vitro* toxicity profile (16, 18). However, no systematic *in vivo* study has been reported on the toxicological profile of *f*-CNT.

More importantly, studies on the identification of the pharmacological profile of i.v. administered CNT are lacking completely. Critical pharmacological parameters such as blood circulation and clearance half-life, organ biodistribution, and accumulation that are essential for the development of any pharmaceutical have yet to be determined. This need is of fundamental importance for the

APPLIED PHYSICAL SCIENCES

MEDICAL SCIENCES

development of novel nanomaterial-based delivery systems for therapeutics (29). In the present work, we are presenting previously unreported data on blood circulation and clearance half-life, as well as tissue biodistribution of two types of radiolabeled functionalized single-walled CNT (*f*-SWNT) after i.v. administration.

Results and Discussion

The ammonium-functionalized CNT (single- and multiwalled) prepared following the 1,3-dipolar cycloaddition method were used to covalently link the diethylentriaminepentaacetic (DTPA) dianhydride (30). This chelating agent allows the complexation of radiometal and/or lanthanide agents such as ^{111}In, which is one of the most common radionuclides used in biodistribution studies of therapeutic molecules (31). The dianhydride form of DTPA readily reacts with CNT **1** (Scheme 1), and the derived DTPA-CNT can be subsequently chelated with [111]In. Two different amounts of DTPA dianhydride were used to (*i*) completely saturate the amino functions on the CNT (**2**) and (*ii*) react only 60% of the amino functions with DTPA (**4**). The quantitative Kaiser test was used to establish the amount of free amino functions around the sidewalls of the nanotubes.

f-CNT were examined and characterized by transmission electron microscopy (TEM). Fig. 1 shows images characteristic of *f*-SWNT and functionalized multiwalled CNT (*f*-MWNT) obtained after dispersion of the sample onto a TEM grid and evaporation of the solvent.

The presence of free amino functions on SWNT **4** allowed for evaluation of the effect of nanotube surface charge distribution on
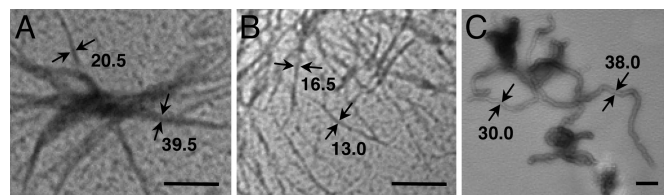
in vivo tissue biodistribution compared with the DTPA-saturated SWNT **2**. Once the DTPA–CNT derivatives **2** and **4** were isolated and characterized (Table 1), they were complexed with [111]In. Both types of DTPA–SWNT were incubated in a solution of [^{111}In]citrate to generate, upon chelation, a final radioactivity load of 20 μCi (1 Ci = 37 GBq) for 60 μg of conjugate, which was the dose of [^{111}In]DTPA–SWNT administered to each animal. As a consequence, one indium isotope was caged in every $\approx$70,000 or $\approx$42,000 DTPA moiety at the surface of nanotubes **3** and **5**, respectively. The complexation reaction was extremely efficient, and the chelating agent caged the radionuclide. We verified that CNT did not cause any reduced or incomplete chelation of the indium. For this purpose, we prepared a DTPA derivative by reacting DTPA dianhydride with the amino acid phenylalanine. The derivative could be easily characterized by HPLC alone and complexed to the indium. The efficiency of the DTPA–(Phe-NH_2)$_2$ agent was measured by incubation with different amounts of indium. In particular, the completeness of indium chelation using a ratio of 2:1 DTPA–(Phe-NH_2)$_2$ to indium was evaluated. This ratio is much lower than that used to chelate ^{111}In on the SWNT (70,000:1 or 42,000:1). Subsequently, DTPA–SWNT were incubated with indium in a 2:1 molar ratio. After 1 h, DTPA–(Phe-NH_2)$_2$ was added, and the solution was analyzed by HPLC. No trace of [In]DTPA–(Phe-NH_2)$_2$ was detected as a consequence of a complete chelation of the indium by the DTPA–SWNT. We also incubated the SWNT **1** devoid of the DTPA group with indium, and after 1 h we added DTPA–(Phe-NH_2)$_2$ to completely recover the [In]DTPA–(Phe-NH_2)$_2$ complex. These experiments indicated that our DTPA–SWNT conjugate is extremely efficient in chelating the radioisotope for the biodistribution studies.

We then compared the tissue distribution and affinity over time after i.v. injection of [^{111}In]DTPA–SWNT **3**, which possess no free amino groups, with that of [^{111}In]DTPA–SWNT **5**, which possess 40% of free amino groups (Table 1) and, therefore, a different

Fig. 1. TEM images of single-walled (*A* and *B*) and multiwalled (*C*) DTPA–CNT. Highly water-soluble and homogeneously dispersed DTPA–CNT were deposited on a TEM grid for observation. (*A* and *B*) DTPA–SWNT form bundles of different length and diameters. Black arrows indicate the dimensions of SWNT bundles, each consisting of 10 and 40 tubes. The thickness of the bundles is in nm. (*C*) DTPA–MWNT were imaged as individual tubes with diameters $\approx$30–38 nm as indicated by the black arrows. (Scale bars, 200 nm.)

Table 1. [^{111}In]DTPA–CNT characteristics

f-CNT	Initial NH_3^+ loading,* mmol/g	DTPA loading,* mmol/g	Free NH_3^+,* mmol/g	DTPA/[^{111}In] ratio
3	0.5	0.5	0	$\approx$70000:1
5	0.5	0.3	0.2	$\approx$42000:1

*Determined by the quantitative Kaiser test.

Singh *et al.*

Table 2. [¹¹¹In]DTPA–CNT 5 and [¹¹¹In]DTPA–CNT 3 percentage of injected dose per gram of tissue after i.v. administration

Organ	30 min		3 h		24 h	
	Mean % dose per g	SD	Mean % dose per g	SD	Mean % dose per g	SD
[¹¹¹In]DTPA–CNT **5**						
Blood	3.1648	1.9622	0.0665	0.0015	0.0137	0.0134
Bone	4.6303	7.0080	0.0510	0.0721	—	0
Heart	0.5228	0.2723	0.0051	0.0014	0.0006	0.0009
Kidney	20.7299	25.6799	0.8707	0.1570	0.6649	0.1411
Liver	0.1984	0.0636	0.1050	0.0232	0.0772	0.0074
Lung	1.3456	0.7871	0.0020	0.0028	—	—
Muscle	8.5542	14.1477	0.0066	0.0093	—	—
Skin	9.0763	10.2912	0.0982	0.0155	0.1124	0.0069
Spleen	0.2233	0.0951	0.1348	0.0362	0.0020	0.0035
[¹¹¹In]DTPA–CNT **3**						
Blood	2.6577	1.5944	0.1588	0.1217	0.0260	0.0185
Bone	6.2041	7.2225	0.4079	0.2538	0.0753	0.0835
Heart	0.2163	0.2080	0.0455	0.0417	0.0015	0.0027
Kidney	10.5797	12.5324	0.7083	0.9538	0.4728	0.1979
Liver	0.1874	0.0600	0.1733	0.0030	0.1118	0.0560
Lung	0.4656	0.2181	0.0464	0.0319	0.0119	0.0092
Muscle	6.1598	8.9923	0.0842	0.0352	0.0003	0.0005
Skin	1.9102	1.7001	0.1726	0.0499	0.1643	0.1660
Spleen	0.4213	0.3533	0.0460	0.0002	—	—

surface-charge distribution. Similar to numerous cationic molecules, such as cationic lipids, which are used to condense plasmid DNA for gene delivery and are known to have many interactions with blood proteins which may affect their pharmacokinetics (32, 33), we hypothesized that evaluation of the effect of charge on nanotube biodistribution is an important parameter toward the development of *f*-CNT for systemic gene delivery.

We were able to detect the presence of both types of the *f*-SWNT in all of the organs examined 30 min after administration, with the higher levels of radioactivity found in the muscle, skin, kidney, and blood (Tables 2 and 3) for both types of nanotubes. Interestingly, although it appears that after 30 min the [¹¹¹In]DTPA–CNT **5** may be found in the kidney, muscle, skin, and lung at slightly higher affinity than [¹¹¹In]DTPA–CNT **3**, in both cases the nanotubes are

rapidly cleared from all tissues (Fig. 2). A closer examination of the tissue affinity data indicates that ≈20% of the injected dose of nanotubes can be found per gram of tissue in the kidneys of mice administered [¹¹¹In]DTPA–SWNT **5** after 30 min, with 8.5% in the muscle, 9% in the skin, and 1.3% in the lungs (Table 2). By comparison, the tissue affinity of [¹¹¹In]DTPA–CNT **3** after 30 min is 10.5% in the kidney, with ≈6% in the muscle, 2% in the skin, and <0.5% found in the lung.

The high levels of ¹¹¹In found in the kidney after 30 min and the rapid decline in the overall radioactivity levels thereafter indicate that most of the nanotubes are eliminated through the renal excretion route. A simple calculation from the data presented in Table 3 indicates that after 3 h, <1% of [¹¹¹In]DTPA–CNT **3** is detectable in all organs measured, falling to <0.7% after 24 h. A

Table 3. [¹¹¹In]DTPA–CNT 5 and [¹¹¹In]DTPA–CNT 3 percentage of injected dose per organ after i.v. administration

| Organ	30 min		3 h		24 h	
	Mean % dose per organ	SD	Mean % dose per organ	SD	Mean % dose per organ	SD
[¹¹¹In]DTPA–CNT **5**						
Blood	4.5182	2.7105	0.2699	0.2069	0.0442	0.0314
Bone	0.2215	0.2354	0.0166	0.0147	0.0030	0.0027
Heart	0.0275	0.0230	0.0039	0.0032	0.0002	0.0004
Kidney	2.4806	3.1174	0.1840	0.1431	0.1417	0.0459
Liver	0.1784	0.0686	0.1655	0.0237	0.1040	0.0544
Lung	0.0897	0.0620	0.0036	0.0018	0.0016	0.0012
Muscle	49.2787	71.9382	0.6740	0.2814	0.0022	0.0038
Skin	7.6407	6.8005	0.6903	0.1996	0.6572	0.6642
Spleen	0.0375	0.0280	0.0037	0.0002	—	—
[¹¹¹In]DTPA–CNT **3**						
Blood	5.3802	3.3357	0.1130	0.0026	0.0233	0.0227
Bone	0.3124	0.4894	0.0021	0.0030	—	—
Heart	0.0483	0.0221	0.0006	0.0002	0.0001	0.0001
Kidney	4.7936	5.5527	0.2262	0.0577	0.1303	0.0260
Liver	0.1693	0.0319	0.1144	0.0396	0.0773	0.0117
Lung	0.1326	0.0428	0.0002	0.0003	—	—
Muscle	68.4333	113.1819	0.0528	0.0747	—	—
Skin	36.3054	41.1663	0.3930	0.0620	0.4495	0.0277
Spleen	0.0327	0.0034	0.0064	0.0038	0.0001	0.0001

APPLIED PHYSICAL SCIENCES

MEDICAL SCIENCES
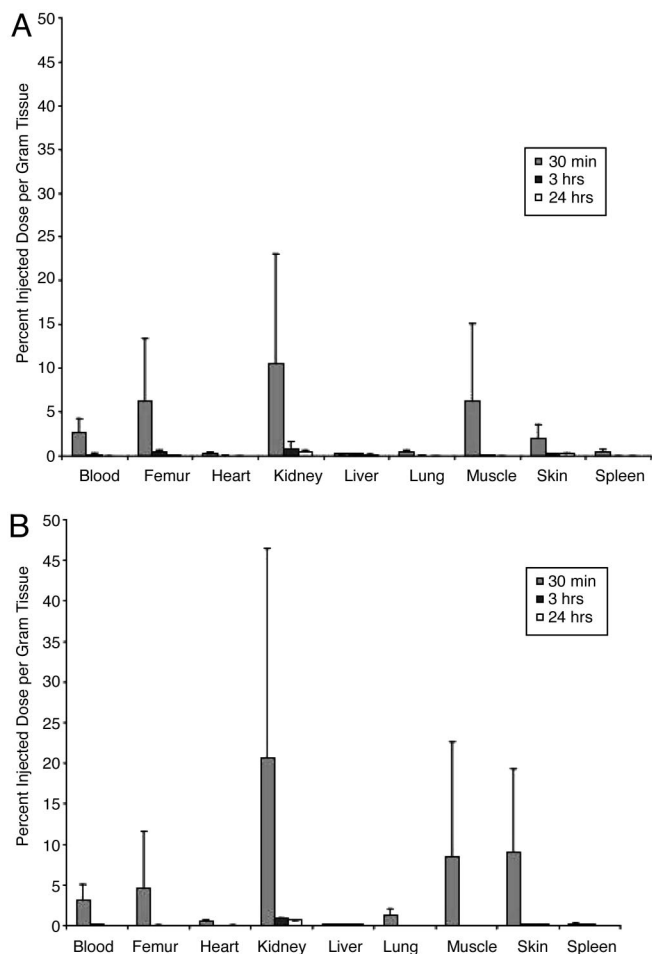
Fig. 2. Biodistribution per collected gram of tissue of [^{111}In]DTPA–SWNT **3** (*A*) and [^{111}In]DTPA–SWNT **5** (*B*) after i.v. administration.

Fig. 3. TEM images of excreted urine samples containing single- and multiwalled DTPA–CNT. The urine samples were centrifuged, and both the supernatant and the precipitate were analyzed. (*A* and *B*) DTPA–SWNT from the supernatant. (Scale bars, 500 nm.) (*C–E*) DTPA–MWNT into the supernatant. (*F–H*) DTPA–MWNT in the precipitate. (Scale bars for *C–H*, 100 nm.)

similar rapid decline in percent dose of nanotubes remaining can be observed with the [^{111}In]DTPA–CNT **5** because <2% of the injected dose remains after 3 h before falling to <1%. The differences between the two types of tubes are not considered statistically significant.

After this biodistribution study, we carried out an *in vivo* excretion study to investigate the presence of *f*-SWNT and *f*-MWNT in the excreted urine. *f*-MWNT were included to examine whether i.v. administered CNT of larger dimensions compared with *f*-SWNT (Fig. 1) were excreted in urine. Doses of 400 μg of DTPA–SWNT **4** and DTPA–MWNT **4** were administered i.v., and urine was collected within an 18-h period after administration. All animals exhibited no signs of acute toxicity after administration even at these higher CNT doses. TEM analysis of urine samples indicated the abundant presence of intact *f*-SWNT and *f*-MWNT (Fig. 3). These observations confirmed that both *f*-SWNT and *f*-MWNT are cleared from systemic blood circulation through the renal excretion route and into urine as intact nanotubes.

In contrast to Wang *et al.* (34), who examined the organ distribution of carboxylated CNT after i.p. administration and observed some accumulation in bone, we did not see any organ-specific accumulation of i.v. administered nanotubes over time. None of the animals in our studies exhibited any signs of renal or other severe acute toxicity responses; however, more systematic toxicological studies need to be performed. Radioactive tracer studies similar to ours (35) that determined the biodistribution of functionalized fullerenes (buckyballs), which were far smaller than
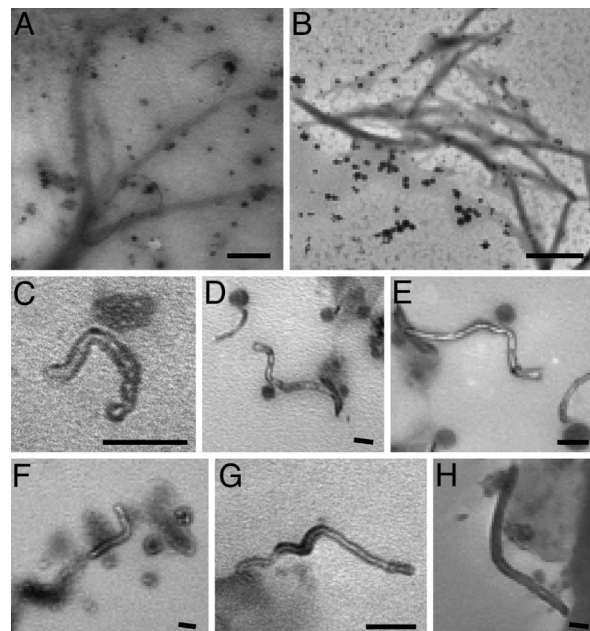
the nanotubes used here, indicated that these smaller fullerenes had varying affinities for the liver, spleen, bone, and kidney, depending on the functional group. Carboxylic acid functionalized fullerenes exhibiting high levels of retention were observed even 48–72 h after i.v. administration, whereas hydroxyl-functionalized fullerenes were rapidly excreted through urine for both rats and rabbits (35–37). More interestingly, it was reported that carboxyl-functionalized fullerenes were able to penetrate the blood-brain barrier, contrary to hydroxyl-functionalized fullerenes, which did not.

Such observations have direct implications for the use of carbon-based nanomaterials as delivery systems and highlight the importance of the type of functionalization on the pharmacokinetic and tissue biodistribution profile obtained. The lack of any organ-specific affinity for the nanotubes in the present study can be considered an advantage for the development of targeted nanotubes, because there is no innate tissue affinity to overcome. Importantly, liver accumulation and hepatic toxicity has previously rendered many delivery systems ineffective; however, *f*-CNT-based delivery systems may offer an alternative because no inherent liver accumulation is observed.

Finally, to further elucidate the pharmacokinetic profile of the functionalized nanotubes, we calculated the blood clearance rates of the two types of radiolabeled *f*-SWNT (Fig. 4). [^{111}In]DTPA–SWNT **5** have a blood circulation half-life of ≈3 h, and [^{111}In]DTPA–SWNT **3** have a half-life of just over 3.5 h. To our knowledge, such a calculation has not been made previously for any kind of CNT administered *in vivo*. Because the cationic *f*-SWNT have already been demonstrated to be capable of delivering plasmid DNA to cells *in vitro* (18, 38), this work is an important step toward the development of such nanotubes for systemic gene transfer.

To put these rates in context with other commonly used gene therapy vectors, <10% of i.v. injected adenovirus can be found in the blood as little as 10 min after i.v. injection, falling to <1% after 1 h, representing a blood clearance half-life of only 2 min (39). Cationic lipoplexes are cleared even more rapidly, with only 10% of the injected dose of some formulations remaining detectable in the blood as little as 1 min after i.v. injection (40). Polyplexes formed
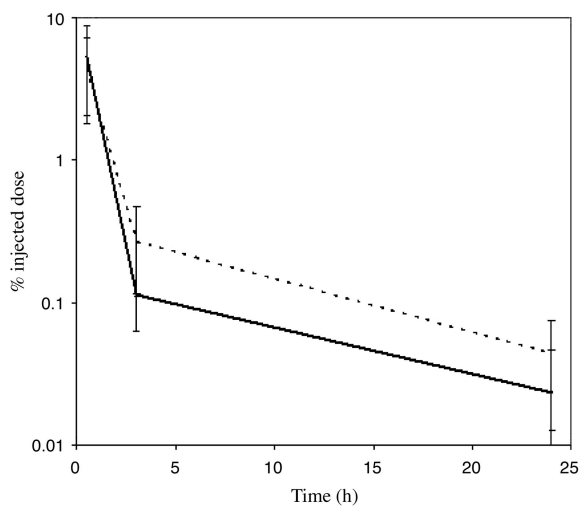
Fig. 4. Blood circulation of ^{111}In-radiolabeled CNT. The graph represents the percentage of injected dose at different time points. i.v. injection of *f*-SWNT **3** (solid black line; $t_{1/2}$ = 3.52 ± 1.59) and i.v. injection of *f*-SWNT **5** (short dotted black line; $t_{1/2}$ = 2.99 ± 1.59) are shown. The trend presented is close to the exponential elimination profile if corrected by the standard deviation (SD). Half-life was calculated on the basis of the corresponding concentration–time data determining the elimination constant and applying the equation $t_{1/2}$ = ln2/K_{el}. After five half-lives, CNT are not present at all in the blood. Half-life SD was calculated by using $\sigma = |\sigma_{x_1}|/x_1 + |\sigma_{x_2}|/x_2$ where x_1 and x_2 are the calculated percentage of injected dose at time 30 min and 24 h, and σ is the related SD.

from polylysine–DNA complexes are cleared from circulation between 5 (41) and 30 (42) minutes.

Conversely, the blood circulation half-life of the *f*-CNT in this study is significantly shorter than that of other functionalized C_{60} fullerenes, which have been shown to have a blood half-life of 6.8 h after i.v. administration (43). These fullerenes do not appear to be excreted through the urine and seem to have a high level of affinity for plasma proteins. Perhaps the short blood half-life of the i.v. injected nanotubes in the present study is an indication of low interaction with blood proteins.

Conclusions

We observed that surface charge density differences of functionalized, water-soluble, and ^{111}In-labeled DTPA–SWNT do not alter their tissue selectivity, because both types studied followed a rapid, first-order clearance from the blood compartment through the renal excretion route without any toxic side effects or mortality. Furthermore, we were able to visualize intact *f*-SWNT and *f*-MWNT in excreted urine. These observations are important as a further indication that functionalized, and thereby water-soluble and biocompatible, carbon nanomaterial exhibit a significantly improved toxicity profile compared with their nonfunctionalized counterparts. The [^{111}In]DTPA–SWNT **5**, carrying free ammonium groups included in this study, also can be used to complex and deliver nucleic acids across mammalian cell surfaces, offering the possibility for systemic gene transfer. This work presents previously undescribed pharmacokinetic data after i.v. administration of CNT, exhibiting a blood circulation half-life of up to 3.5 h. It is hoped that this work can act as an impetus for further pharmacological investigations of different types of nanotubes to determine the limitations and opportunities CNT-based delivery systems offer.

Materials and Methods

SWNT were purchased from Carbon Nanotechnologies Inc. (Houston). Pristine SWNT used in this experiment were CNI Grade/Lot No. R0496. According to the manufacturer, the mean diameter of

SWNT is ≈1 nm. Tubes have lengths between 300 and 1,000 nm. However, the more accurate SWNT length determination after functionalization is a topic of intensive current research because the dispersed tubes organize themselves into ropes. MWNT were purchased from Nanostructured & Amorphous Materials Inc. (Houston). MWNT used in this study were 94% pure (stock no. 1240XH). Their outer diameter was between 20 and 30 nm, and length was between 0.5 and 2 μm. The dimensions and structure of the CNT obtained after functionalization used in this study are shown in Fig. 1. DTPA was selected as the chelating agent, because it has been widely used to chelate different types of radioelements, currently used in radiology clinics. It is commercially available (Aldrich), highly water-soluble, and allows for a simple conjugation chemistry through linkage to the amino functions at the CNT surface. Also, DTPA rapidly cages indium with a highly thermodynamic equilibrium constant (44). The radioactive tracer [^{111}In]Cl$_3$ was obtained from Amersham Pharmacia Biosciences as an aqueous solution and used without further purification. Radioactive ^{111}In has a decay half-life of 67.5 h, convenient for biodistribution studies.

Preparation of DTPA–SWNT 2. SWNT **1,** prepared as reported in ref. 30 (4.0 mg; 2.0 μmol), was dissolved in 500 μl of DMSO and neutralized with diisopropylethylamine (DIEA) (1 μl; 5.9 μmol). DTPA dianhydride (714 μg; 2.0 μmol) was added. The mixture was stirred for 3 h at room temperature. The DMSO solution was diluted with water (5 ml) and lyophilized twice. The crude DTPA–CNT derivative was reprecipitated from methanol/diethyl ether several times and lyophilized again from water. The reaction was complete as confirmed by a negative Kaiser test. SWNT **2** was obtained as a brown powder, ready for complexation with the radionuclide.

Preparation of DTPA–SWNT 4 and DTPA–MWNT 4. SWNT **1,** prepared as reported in ref. 30 (5.5 mg; 2.75 μmol), was dissolved in 1 ml of DMSO and neutralized with diisopropylethylamine (DIEA) (1 μl; 5.9 μmol). DTPA dianhydride (590 μg; 1.65 μmol) was added, and the mixture was stirred for 3 h at room temperature. The DMSO solution was diluted with water (10 ml) and lyophilized twice. The crude DTPA–CNT derivative was reprecipitated from methanol/diethyl ether several times and lyophilized again from water. The number of the free amino groups remaining on the CNT was measured by the quantitative Kaiser test. According to the ratio between the number of amino functions on CNT **1** and the amount of DTPA used, 40% of amines remained unreacted. Compound **4** was obtained as a brown powder, ready for complexation with the radionuclide. The synthesis of DTPA–CNT **4** was repeated with MWNT using 4 mg (3.2 μmol) of ammonium-functionalized MWNT (loading: 0.8 mmol/g), prepared as reported in ref. 30, and 972 μg (2.72 μmol) of DTPA dianhydride in 1 ml of DMSO. According to the quantitative Kaiser test, 15% of amine groups remained free at the end of this reaction.

Synthesis of Radiotracer [^{111}In]DTPA–CNT 3 and 5. [^{111}In]DTPA–CNT (single-walled) was obtained by cationic exchange from a solution of [^{111}In]citrate. A 3% sodium citrate water solution (150 μl) was added to 50 μl of a sterile solution of [^{111}In] chloride in 0.04 M hydrochloric acid (10 mCi/ml). After 30 min, 37.5 μl of a sterile water solution of **2** or **4** (4 mg in 100 μl) was added and allowed to react for 1 h at room temperature under gentle hand-shaking. The reaction volume was increased to a final volume of 5 ml with sterile PBS. The obtained [^{111}In]DTPA–CNT **3** or **5** solution was directly injected into the mice without further treatment.

Synthesis of DTPA–(Phe-NH$_2$)$_2$. Rink amide resin (NeoMPS, Strasbourg, France) (300 mg; 213 μmol) was initially treated with a solution of 25% piperidine in dimethylformamide (DMF) to remove the fluorenylmethoxycarbonyl (Fmoc) group. Subsequently,

Fmoc–Phe–OH (5 equiv) in DMF (6 ml) was added in the presence of Bop/HOBt/diisopropylethylamine (DIEA) (5/5/15 equiv). The coupling was repeated twice for 20 min. After washings, Fmoc was removed by using a solution of 25% piperidine in DMF. DTPA dianhydride (228 mg; 3 equiv) was added in DMF (5 ml). The reaction was shaken for 15 h, and the resin was washed. The compound was removed from the resin with pure trifluoroacetic acid (TFA) for 24 h and precipitated with cold diethyl ether. After lyophilization, a white powder (74 mg) was recovered. Yield: 93%. HPLC: R_T 9.01 min (0–100% of B in 20 min. A: $H_2O/0.1\%TFA$; B: ACN/0.08%TFA) MALDI-TOF: (m/z) calculated, 685.72; found, 686.19 $[M+H]^+$. ^1H NMR (300 MHz, DMSO): δ (ppm) 8.24, 7.56, 7.20, 4.51, 4.07, 3.4–2.7. ^{13}C NMR (75 MHz, DMSO): δ (ppm) 173.25, 172.49, 170.27, 138.39, 129.60, 128.55, 126.76, 56.43, 55.12, 54.25, 51.75, 49.54, 38.09.

Biodistribution Studies. Female 6- to 8-week-old BALB/c mice were purchased from Charles River Laboratories. Studies were conducted with prior approval from the UK Home Office. A total of 18 mice were used, 9 per material with three per time point. Mice were injected via the tail vein with 200 μl of PBS containing 60 μg of $[^{111}In]DTPA–CNT$ **3** or $[^{111}In]DTPA–CNT$ **5**. Each injection contained 20 μCi of ^{111}In activity. At 30 min, 3 h, and 24 h after injection, three mice per group were killed, blood was collected, and then the animal was flushed with 10 ml of normal saline via the heart to clear any blood remaining in other organs. Muscle (left thigh), bone (left femur with marrow), skin, heart, lung, liver, kidney, and spleen were collected and placed into preweighed scintillation vials. Each organ was then weighed, and samples were analyzed for ^{111}In activity using a PerkinElmer (Packard) Cobra II gamma counter. Chelation of ^{111}In with DTPA and other chelating agents form very stable complexes that are commonly used for *in vivo* biodistribution studies of various therapeutic molecules and

their delivery systems (45–47). The stability constant between DTPA and ^{111}In has been determined by others to be 1.5×10^{29} (48), and previous studies have shown that the $[^{111}In]$–DTPA ligand has a strong chelating effect on the radiometal in human serum (44). Moreover, we characterized the In–DTPA complex using nonradioactive indium by HPLC without any loss of indium, concluding that the chelate is stable under physiological conditions.

Excretion Studies and Urine Microscopic Analysis. Female, 8-week-old BALB/c mice were purchased from Harlan Olac (Bichester, U.K.). Studies were conducted with prior approval from the UK Home Office. Mice were injected via the tail vein with 200 μl of PBS containing 400 μg of DTPA–SWNT **4**. For comparison, separate groups of mice were injected with 200 μl of PBS containing 400 μg of DTPA–MWNT **4**. As a control, four mice were injected with 200 μl of PBS alone. Groups of four mice were placed in metabolic cages (Tecniplast UK, Kettering Northants, U.K.), and urine was collected over 18 h. After collection of urine, a sample of 100 μl from each group was lyophilized. The pellet obtained was dispersed in methanol or water (2 mg/ml) and centrifuged (15,000 rpm on a Biofuge 13, Heraeus). The precipitate after centrifugation was resuspended in 100 μl of water. Both supernatant and precipitates from each urine sample were analyzed microscopically using TEM.

1. Kroto, H. W., Heath, J. R., O'Brien, S. C., Curl, R. F. & Smalley, R. E. (1985) *Nature* **318,** 162–163.
2. Iijima, S. (1991) *Nature* **354,** 56–58.
3. Dresselhaus, M. S., Dresselhaus, G. & Eklund, P. C. (1996) *Science of Fullerenes and Carbon Nanotubes* (Academic, New York).
4. Milne, W. I., Teo, K. B. K., Amaratunga, G. A. J., Legagneux, P., Gangloff, L., Schnell, J. P., Semet, V., Binh, V. T. & Groening, O. (2004) *J. Mater. Chem.* **14,** 933–943.
5. Patchkovskii, S., Tse, J. S., Yurchenko, S. N., Zhechkov, L., Heine, T. & Seifert, G. (2005) *Proc. Natl. Acad. Sci. USA* **102,** 10439–10444.
6. Weisman, R. B. (2003) *Nat. Mater.* **2,** 569–570.
7. Service, R. F. (2003) *Science* **302,** 1310.
8. Javey, A., Guo, J., Wang, Q., Lundstrom, M. & Dai, H. (2003) *Nature* **424,** 654–657.
9. Wong, S. S., Joselevich, E., Woolley, A. T., Cheung, C. L. & Lieber, C. M. (1998) *Nature* **394,** 52–55.
10. Hirsch, A. (2002) *Angew. Chem. Int. Ed.* **41,** 1853–1859.
11. Bianco, A., Kostarelos, K., Partidos, C. D. & Prato, M. (2005) *Chem. Commun.*, 571–577.
12. Williams, K. A., Veenhuizen, P. T., de la Torre, B. G., Eritja, R. & Dekker, C. (2002) *Nature* **420,** 761.
13. Chen, R. J., Bangsaruntip, S., Drouvalakis, K. A., Kam, N. W., Shim, M., Li, Y., Kim, W., Utz, P. J. & Dai, H. (2003) *Proc. Natl. Acad. Sci. USA* **100,** 4984–4989.
14. Kam, N. W. S., O'Connell, M., Wisdom, J. A. & Dai, H. J. (2005) *Proc. Natl. Acad. Sci. USA* **102,** 11600–11605.
15. Park, K. H., Chhowalla, M., Iqbal, Z. & Sesti, F. (2003) *J. Biol. Chem.* **278,** 50212–50216.
16. Pantarotto, D., Briand, J. P., Prato, M. & Bianco, A. (2004) *Chem. Commun.*, 16–17.
17. Pantarotto, D., Partidos, C. D., Hoebeke, J., Brown, F., Kramer, E., Briand, J. P., Muller, S., Prato, M. & Bianco, A. (2003) *Chem. Biol.* **10,** 961–966.
18. Pantarotto, D., Singh, R., McCarthy, D., Erhardt, M., Briand, J. P., Prato, M., Kostarelos, K. & Bianco, A. (2004) *Angew. Chem. Int. Ed.* **43,** 5242–5246.
19. Maynard, A. D., Baron, P. A., Foley, M., Shvedova, A. A., Kisin, E. R. & Castranova, V. (2004) *J. Toxicol. Environ. Health A* **67,** 87–107.
20. Huczko, A. & Lange, H. (2001) *Fullerene Sci. Technol.* **9,** 247–250.
21. Huczko, A., Lange, H., Bystrzejewski, M., Baranowski, P., Grubek-Jaworska, H., Nejman, P., Przybylowski, T., Czuminska, K., Glapinski, J., Walton, D. R. M. & Kroto, H. W. (2005) *Fullerenes Nanotubes Carbon Nanostruct.* **13,** 141–145.
22. Lam, C. W., James, J. T., McCluskey, R. & Hunter, R. L. (2004) *Toxicol. Sci.* **77,** 126–134.
23. Warheit, D. B., Laurence, B. R., Reed, K. L., Roach, D. H., Reynolds, G. A. M. & Webb, T. R. (2004) *Toxicol. Sci.* **77,** 117–125.
24. Shvedova, A. A., Kisin, E. R., Mercer, R., Murray, A. R., Johnson, V. J., Potapovich, A. I., Tyurina, Y. Y., Gorelik, O., Arepalli, S., Schwegler-Berry, D., *et al.* (2005) *Am. J. Physiol.* **289,** L698–L708.
25. Yokoyama, A., Sato, Y., Nodasaka, Y., Yamamoto, S., Kawasaki, T., Shindoh, M., Kohgo, T., Akasaka, T., Uo, M., Watari, F. & Tohji, K. (2005) *Nano Lett.* **5,** 157–161.
26. Sato, Y., Yokoyamab, A., Shibatab, K.-i., Akimotoa, Y., Oginoa, S.-i., Nodasakab, Y., Kohgob, T., Tamurab, K., Akasakab, T., Uob, M., *et al.* (2005) *Mol. BioSyst.* **1,** 176–182.
27. Sayes, C. M., Fortner, J. D., Guo, W., Lyon, D., Boyd, A. M., Ausman, K. D., Tao, Y. J., Sitharaman, B., Wilson, L. J., Hughes, J. B., *et al.* (2004) *Nano Lett.* **4,** 1881–1887.
28. Sayes, C. M., Liang, F., Hudson, J. L., Mendez, J., Guo, W., Beach, J. M., Moore, V. C., Doyle, C. D., West, J. L., Billups, W. E., *et al.* (2006) *Toxicol. Lett.* **161,** 135–142.
29. Kostarelos, K. (2003) *Adv. Colloid Interface Sci.* **106,** 147–168.
30. Georgakilas, V., Kordatos, K., Prato, M., Guldi, D. M., Holzinger, M. & Hirsch, A. (2002) *J. Am. Chem. Soc.* **124,** 760–761.
31. Anderson, C. J. & Welch, M. J. (1999) *Chem. Rev.* **99,** 2219–2234.
32. Li, S., Tseng, W. C., Stolz, D. B., Wu, S. P., Watkins, S. C. & Huang, L. (1999) *Gene Ther.* **6,** 585–594.
33. Zuhorn, I. S., Visser, W. H., Bakowsky, U., Engberts, J. B. & Hoekstra, D. (2002) *Biochim. Biophys. Acta* **1560,** 25–36.
34. Wang, H. F., Wang, J., Deng, X. Y., Sun, H. F., Shi, Z. J., Gu, Z. N., Liu, Y. F. & Zhao, Y. L. (2004) *J. Nanosci. Nanotechnol.* **4,** 1019–1024.
35. Cagle, D. W., Kennel, S. J., Mirzadeh, S., Alford, J. M. & Wilson, L. J. (1999) *Proc. Natl. Acad. Sci. USA* **96,** 5182–5187.
36. Qingnuan, L., yan, X., Xiaodong, Z., Ruili, L., qieqie, D., Xiaoguang, S., Shaoliang, C. & Wenxin, L. (2002) *Nucl. Med. Biol.* **29,** 707–710.
37. Yamago, S., Tokuyama, H., Nakamura, E., Kikuchi, K., Kananishi, S., Sueki, K., Nakahara, H., Enomoto, S. & Ambe, F. (1995) *Chem. Biol.* **2,** 385–389.
38. Singh, R., Pantarotto, D., McCarthy, D., Chaloin, O., Hoebeke, J., Partidos, C. D., Briand, J. P., Prato, M., Bianco, A. & Kostarelos, K. (2005) *J. Am. Chem. Soc.* **127,** 4388–4396.
39. Alemany, R., Suzuki, K. & Curiel, D. T. (2000) *J. Gen. Virol.* **81,** 2605–2609.
40. Mahato, R. I., Kawabata, K., Takakura, Y. & Hashida, M. (1995) *J. Drug Target* **3,** 149–157.
41. Dash, P. R., Read, M. L., Barrett, L. B., Wolfert, M. A. & Seymour, L. W. (1999) *Gene Ther.* **6,** 643–650.
42. Oupicky, D., Howard, K. A., Konak, C., Dash, P. R., Ulbrich, K. & Seymour, L. W. (2000) *Bioconjugate Chem.* **11,** 492–501.
43. Rajagopalan, P., Wudl, F., Schinazi, R. F. & Boudinot, F. D. (1996) *Antimicrob. Agents Chemother.* **40,** 2262–2265.
44. Jasanada, F., Urizzi, P., Souchard, J. P., Le Gaillard, F., Favre, G. & Nepveu, F. (1996) *Bioconjugate Chem.* **7,** 72–81.
45. Harrington, K. J., Rowlinson-Busza, G., Syrigos, K. N., Uster, P. S., Vile, R. G., Peters, A. M. & Stewart, J. S. (2001) *Int. J. Radiat. Oncol. Biol. Phys.* **50,** 809–820.
46. Laverman, P., Carstens, M. G., Boerman, O. C., Dams, E. T., Oyen, W. J., van Rooijen, N., Corstens, F. H. & Storm, G. (2001) *J. Pharmacol. Exp. Ther.* **298,** 607–612.
47. Froidevaux, S. & Eberle, A. N. (2002) *Biopolymers* **66,** 161–183.
48. Ivanov, P. I., Bontchev, G. D., Bozhikov, G. A., Filossofov, D. V., Maslov, O. D., Milanov, M. V. & Dmitriev, S. N. (2003) *Appl. Radiat. Isot.* **58,** 1–4.